C84

The intrinsic and extrinic apoptotic pathways are independently activated in response to oxidative stress in pancreatic acinar cells

H.K. Baumgartner[1], J.V. Gerasimenko[1], H.L. Ashurst[1], R. Sutton[3], A.V. Tepikin[1], O.H. Petersen[1], A.J. Watson[2] and O.V. Gerasimenko[1]

[1]Physiology, University of Liverpool, Liverpool, UK, [2]Division of Gastroenterology, University of Liverpool, Liverpool, UK and [3]Division of Surgery & Oncology, University of Liverpool, Liverpool, UK

Oxidative stress plays an important role in the pathogenesis of acute pancreatitis. Increased generation of reactive oxygen species is a well known initiator of apoptosis and has been shown to induce apoptosis in mouse pancreatic acinar cells [1]. Opening of the permeability transition pore, release of cytochrome c, and activation of caspase-9 occurs in these cells in response to oxidative stress; however, a small population of cells can still undergo apoptosis when the opening of the permeability transition pore is blocked. We investigated the possible role and mechanism of action of the alternative apoptotic pathways versus the intrinsic pathway in pancreatic acinar cells exposed to oxidant stress.

Mouse pancreatic acinar cells (freshly isolated from CD1 mice) were loaded with a fluorescent substrate for caspase-9 or caspase-8. Using confocal microscopy, fluorescence of cleaved substrate was imaged in real time in response to the oxidant menadione (30 μM). Cells were positive for caspase activation when fluorescence was higher than the average fluorescence of control cells plus two standard deviations. Caspase-9 or caspase-8 activity was examined in control cells and cells pre-treated with 25 μM BAPTA-AM to prevent cytoplasmic calcium elevations, 200 μM TPEN to reduce calcium within the endoplasmic reticulum, 50 μM bongkrekic acid to block opening of the mitochondrial permeability transition pore, 10-40 μM caspase-9 inhibitor, or 50 μM GPN to disrupt lysosomes. An unpaired, two-tailed Student's t test was used for statistical comparisons between treatment groups ($p<0.05$ was significant).

Caspase-9 was activated within a few minutes ($t_{1/2} = 129 \pm 43$ s; n=12) after administration of menadione. Activation of caspase-9 was significantly inhibited in cells pre-treated with BAPTA-AM, but no change was observed in the presence of 200 μM of TPEN (decreased ER calcium content as measured with Mag-Fluo4). Caspase-8 was activated ($t_{1/2}$) within 26 ± 3 min (n=8) after treatment with menadione in 21 ± 3% of cells (n=716). Activation of caspase-8 was not altered by inhibition of the intrinsic apoptotic pathway with bongkrekic acid or caspase-9 inhibitor. Caspase-8 activation was also not changed in the presence of BAPTA-AM. However, caspase-8 activation was significantly reduced when lysosomes of the cells were destroyed with GPN. Both, the intrinsic and in some cells extrinsic apoptotic pathways are rapidly activated in response to oxidative stress in the pancreatic acinar cell. Caspase-9 activation is calcium-dependent, however, does not require for activation full ER calcium stores. Caspase-8 is activated independently of the intrinsic apoptotic pathway and does not require the increase of cytoplasmic calcium. In contrast, caspase-8 requires functional lysosomes for oxidative stress-induced activation in pancreatic acinar cells.

Gerasimenko et al. (2002). *J Cell Science* **115**, 485-497.

Where applicable, the authors confirm that the experiments described here conform with the Physiological Society ethical requirements.

C85

Mechanisms of free radicals generation in neuronal cultures during anoxia and reoxygenation

A.Y. Abramov[1], A. Scorziello[2] and M.R. Duchen[1]

[1]Physiology, UCL, London, UK and [2]Neuroscience, University of Naples Federico II, Naples, Italy

Although it is widely believed that generation of reactive oxygen species (ROS) makes an important contribution to ischaemic injury in the brain, the mechanisms and time course of ROS generation during ischaemia and reperfusion have not been clearly defined. We have used fluorescence imaging techniques to examine the generation of ROS during oxygen glucose deprivation (OGD). Rates of ROS generation were measured using dihydroethidine (Het) in mixed cultures of glia and neurons from rat hippocampus or cortex. Statistical analysis and exponential curve fitting were performed using Origin 7 software. Results are expressed as means ± standard error of the mean (S.E.M.).

In response to OGD with oxygen levels sufficient to cause loss of mitochondrial potential, we detected an early increase in the rate of ROS production occurring after 3-7 min in the majority of neurons (an increase in rate of 1.58-fold; $p<0.05$; n=215). This increase was followed by a prolonged period (lasting 20-25 min) during which rates of ROS generation were reduced to 36±4.3 of the basal rate in cortical cells. This was then followed by a secondary increase in ROS generation starting after 23-35 min of OGD increasing to 2.1-fold of the basal rate of cortical neurons. Reoxygenation increased the rate of ROS production yet again, to 2.56-fold basal rate in hippocampal and 2.89-fold in cortical neurons. Each of these phases of ROS production seems to reflect a different mechanism as each was inhibited by different compounds: the first phase by the protonophore FCCP (1μM, n=155), the delayed secondary phase by the inhibitor of xanthine oxidase, oxypurinol (20 μM, n=165), while the increase in ROS generated upon reoxygenation was blocked by the inhibitor of the NADPH oxidase, DPI (0.5 μM, n=201), and was absent in cells cultured from gp91phox knockout mice. The response to mitochondrial inhibition by 1mM NaCN with 2μg/ml oligomycin was qualitatively similar but quantitatively quite different. Thus, over 10 min after CN/oligomycin application, the rate of ROS generation increased dramatically (3.35-fold in cortical neurons, $p<0.001$; n=78). This was again followed after 10-20 min by a reduction of the rate of ROS production below basal levels (40.4±4.6% of basal rate in hippocampal neurons) to be followed later by a secondary activation of ROS production (3.14-fold, $p<0.001$, in cortical neurons). These data strongly suggest that ROS is generated by three quite distinct processes at different times during OGD and also show that ROS generation by metabolic inhibition in the presence of oxygen (CN) is quite different to ROS generation by OGD. We suggest that early ROS production is derived from the mitochondrial

respiratory chain. Reduction in ROS generation then correlates with collapse of the mitochondrial potential. Once ATP is depleted, generating AMP and hypoxanthine, xanthine oxidase becomes active generating more ROS despite continued hypoxia. ROS generation at reperfusion is primarily due to activation of the NADPH oxidase.

Where applicable, the authors confirm that the experiments described here conform with the Physiological Society ethical requirements.

C86

Expression of ALS-related mutant SOD1 in astrocytes induces functional deficits in motoneuron mitochondria

L. Bilsland[1], N. Nirmalananthan[3], L. Greensmith[3] and M.R. Duchen[2]

[1]Molecular Neuropathobiology, Cancer Research UK, London, UK, [2]Physiology, University College London, London, UK and [3]Sobell Department of Motor Neuroscience and Movement Disorders, University College London, London, UK

Amyotrophic lateral sclerosis (ALS) is a fatal neurodegenerative disease characterised by the selective loss of motoneurons in the spinal cord, brainstem and motor cortex. Despite extensive research, the pathogenic mechanisms underlying motoneuron degeneration are far from understood. However, increasing evidence suggests that alterations in non-neuronal cell function are likely to contribute to the process of motoneuron degeneration (Gong et al. 2000; Pramatarova et al. 2001; Clement et al. 2003). In this study, the influence of glial cell genotype on motoneuron physiology was examined at a cellular level in an *in vitro* co-culture model based on the SOD1 mutation.

Primary motoneurons from wild-type (WT) or transgenic mice carrying the $SOD1^{G93A}$ mutation were plated onto a layer of either WT or mutant $SOD1^{G93A}$ astrocytes. Various aspects of motoneuron physiology were investigated at 7 days *in vitro* using confocal microscopy. Data were analysed using a one-way ANOVA incorporating a Student Newman Keuls multiple comparison test.

Under resting conditions, the expression of mutant $SOD1^{G93A}$ in either neurons or astrocytes was associated with increased spontaneous calcium activity of co-cultured motoneurons. This increase in the frequency of transient elevations in cytosolic calcium, was consistently accompanied by a significant elevation in mitochondrial calcium concentration, $[Ca^{2+}]_m$, in mutant $SOD1^{G93A}$ expressing co-cultures ($p<0.005$; Table 1).

The elevation in $[Ca^{2+}]_m$ alone did not correlate with a change of mitochondrial potential ($\Delta\psi m$). However, mitochondria of either WT or $SOD1^{G93A}$-expressing motoneurons showed a reduction in $\Delta\psi m$ if co-cultured with mutant $SOD1^{G93A}$ expressing astrocytes ($p<0.005$). In contrast, $\Delta\psi m$ in $SOD1^{G93A}$ expressing motoneurons co-cultured with WT astrocytes did not differ from WT co-cultures ($p>0.3$), despite an elevated $[Ca^{2+}]_m$ (Table 1). The presence of mutant $SOD1^{G93A}$-expressing astrocytes was associated with functional alterations in mitochondrial redox state in co-cultured motoneurons, as measured by NADH autofluorescence (Table 1), indicating impaired respiration, which may mediate the mitochondrial depolarisation observed in these co-cultures.

These results suggest that the expression of mutant $SOD1^{G93A}$ in astrocytes has a significant impact on mitochondrial function of motoneurons. This alteration in mitochondrial function may increase the intrinsic vulnerability of motoneurons to the neurotoxic mechanisms proposed to be involved in ALS pathogenesis.

Table 1

	WTnWTa	SODnWTa	WTnSODa	SODnSODa
% of motoneurons showing spontaneous cytosolic calcium activity	20.6	31.1	19.2	36.8
$[Ca^{2+}]_m$ (rhod-5N fluorescence, arbitrary units)	305.9 ± 4.6	437.9 ± 18.7	376.5 ± 10.2	497.3 ± 9.7
$\Delta\psi m$ (TMRM fluorescence, arbitrary units)	2147.6 ± 392.8	2294.2 ± 401.5	587.1 ± 219.8	453.6 ± 65.7
Mean increase in NADH autofluorescence in response to mitochondrial inhibition (arbitrary units)	1092.7 ± 183.3	1067.4 ± 205.3	707.1 ± 177.0	463.4 ± 71.1

n, neurons; a, astrocytes.

Gong YH et al. (2000). *J Neurosci* **20**, 660-665.

Pramatarova A et al. (2001). *J Neurosci* **21**, 3369-3374.

Clement AM et al. (2003). *Science* **302**, 113-117.

This work was supported by The Wellcome Trust and The Brain Research Trust.

Where applicable, the authors confirm that the experiments described here conform with the Physiological Society ethical requirements.

C87

Disruption of myofibril organisation in the zebrafish mutant relaxed which lacks the dihydropyridine receptor β1a subunit

R. Ashworth

School of Biological and Chemical Sciences, Queen Mary University of London, London, UK

Correct skeletal muscle function is essential for coordinated movement. The foundations of the skeletal muscle system are established in the embryo. Our previous studies have demonstrated a role for nerve activity in the regulation of myofibril organisation during zebrafish embryogenesis [1]. Homozygous zebrafish embryos of the relaxed (*red*^{ts25}) mutant line are paralysed and die within days after hatching. The line carries a mutation in the β1a subunit of the voltage gated calcium channel, the dihydropyridine receptor, which is not expressed [2]. In the present study, we examined slow muscle fibre (adaxial cells) development in relaxed mutants, using whole mount immunocytochemistry. By 24 hours post fertilisation (hpf) adaxial cells had elongated and migrated to the lateral surface of the somite in both mutant and wild type embryos (n=4); a result indicative that calcium signalling via L-type calcium channel is not involved in these processes. In the wild type embryos the myofibrils are packed together into longitudinal bundles to form fibres, whilst in the mutant embryos myofibrils are not aligned laterally and appear disorganised. Previously we have shown that myofibril length was significantly increased relative to somite width in embryos from the *nic1*^{b107} line, which carries a mutation in the α-subunit of the nicotinic acetylcholine receptor. Here

we report an apparent increase in the myofibril length of relaxed mutants (1.06±0.04 n=12 at 24 hpf and 1.08±0.06 n=12 at 48 hpf) compared to wild type embryos (1.03±0.04 n=12 at 24 hpf and 1.06±0.03 n=12 at 48 hpf). We conclude that calcium signalling via dihydropyridine receptors has a role in myofibril organisation during embryogenesis.

Brennan C, Mangoli M, Dyer CE & Ashworth R (2005). J Cell Sci 118, 5181-5190.

Schredelseker J, Di Biase V, Obermair GJ, Felder ET, Flucher BE, Franzini-Armstrong C & Grabner M (2005). Proc Natl Acad Sci U S A 102, 17219-17224.

Funded by BBSRC.

Where applicable, the authors confirm that the experiments described here conform with the Physiological Society ethical requirements.

PC176

Hyposmotic cell swelling promotes cell division

J.E. Parker, T.J. Jacob and S.K. Hall

School of Biosciences, Cardiff University, Cardiff, UK

During cell cycle progression, cells increase in size and must pass a size-dependent checkpoint prior to mitosis. Once a cell has passed this restriction point, it is committed to one cycle of division. Swelling could act as a proliferative signal through activation of cytoplasmic signalling cascades and gene transcription [1]. Mitogen activated protein kinases (MAPK) are central components of the signalling pathways involved in cell cycle progression. Previous studies from this laboratory have demonstrated a rapid early increase in ERK-1,2 activity in chick myocytes following hyposmotically-induced swelling [2]. Such MAPK activation could provide a link between swelling and proliferation.

Embryonic chick hearts were removed at day 10 of development; myocytes were isolated enzymatically and maintained in culture. These cells may undergo at least one further cycle of cell division before terminal differentiation. Reducing extracellular osmolarity causes a significant increase in cell volume; e.g. cell volume increases to ~140% in hyposmotic solution (180 mosmol/l), before regulatory volume decrease occurs [2]. In this study, volume was perturbed by alteration of the extracellular osmolarity (150-400 mosmol/l by omission or addition of mannitol from the culture medium) for up to 48 hours. Cell proliferation was monitored by spectrophotometric assay of the number of viable cells [3]. Statistical comparison of absorbance between experimental groups was performed using one-way ANOVA and post-hoc Tukey tests; significant differences were accepted if $p<0.05$.

Our results demonstrate that cells exposed to hyposmotic media (200mosmol/l) showed a rapid early increase in proliferation, compared to control cultures (Fig. 1). The absorbance was significantly increased, relative to controls at 24 h (0.172±0.071; n=9 wells cf. 0.001±0.004; n=6) and 48 h (0.300±0.095; n=12 cf. 0.048±0.033; n=8). In contrast, cells incubated in hyperosmotic media (400mosmol/l; n=2 experiments) failed to proliferate. Similarly, cells treated with the MEK inhibitor PD98059 (50μM) also failed to proliferate in hyposmotic media (n=2 experiments). This study establishes a link between hyposmotically induced cell swelling and an increase in cell proliferation, and suggests a role for ERK1,2 signalling in swelling-induced mitosis. These data demonstrate that inducing changes in cell size may accelerate or halt progression through the cell cycle.

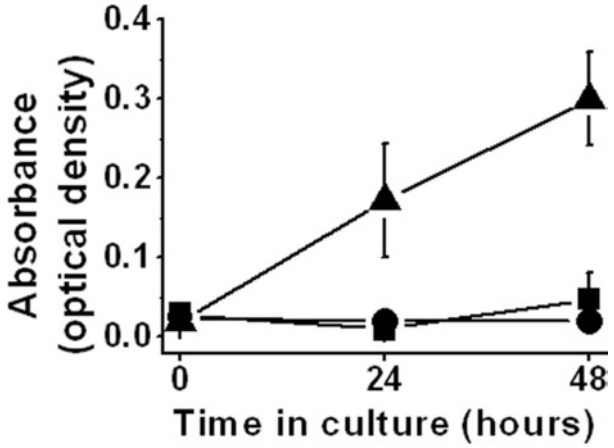

Figure 1. Cell swelling in hyposmotic media causes proliferation

Circles, culture medium (300mosmol/l); triangles, hyposmotic media (200mosmol/l); squares, isosmotic media (300mosmol/l; hyposmotic media + mannitol). Data shown as mean±sem of absorbance; n≥5 wells at each data point.

Kim RD, Stein GS & Chari RS (2001). J Cell Biol 83, 56-69.

Hall SK & Assender JW (2001). J Physiol 536P, 106.P.

Doyle A & Stacey G (2000). In Encyclopedia of Cell Technology, Vol. 1, ed Spier RE, pp. 285-293. John Wiley & Sons Inc., NY.

Where applicable, the authors confirm that the experiments described here conform with the Physiological Society ethical requirements.

PC177

Ca^{2+} oscillations cause a rise in intracellular ATP in fertilizing mouse eggs

K. Campbell and K. Swann

Obstetrics and Gynaecology, Cardiff University, Cardiff, UK

A series of prolonged intracellular Ca^{2+} oscillations are responsible for activating the development of mammalian eggs (Stricker, 1999). These Ca^{2+} oscillations have been shown to cause increases in mitochondrial NADH and FADH2 (Dumollard et al. 2004), but the effects upon cytosolic ATP levels are unclear. Here, we have monitored both intracellular Ca^{2+}, using Oregon Green BAPTA dextran fluorescence, and ATP concentrations using luminescence from firefly luciferase. These indicators were microinjected into mouse eggs and both fluorescent and luminescent images were collected by using a cooled intensified CCD camera based system that allowed for intermittent fluorescent excitation. Data are presented as the mean and SD. During *in vitro* fertilization of mouse eggs we found that Ca^{2+} oscillations were associated with a two-phase rise in luciferase luminescence (131±9.8% for the 1st phase and 161±18.8% for the 2nd phase, n=34). Both increases were significantly different from luminescence levels recorded over a similar time period in unfertilized eggs (unpaired t test, $P<0.005$). This suggests a twofold increase in ATP levels at fertilization from 1.88mM to a peak of 3.02mM. The initial ATP increase started during the first Ca^{2+} transient at fertilization and peaked 30 min after oscillations

began. The secondary increase in ATP typically occurred 1 h after the start of Ca^{2+} oscillations and was inhibited by nocodazole which blocks meiotic resumption (n=12). The ATP levels slowly returned to prefertilization levels after the cessation of Ca^{2+} oscillations. The ATP increase at fertilization was dependent upon Ca^{2+} because fertilization of eggs that had been injected with the Ca^{2+} chelator BAPTA (n=9) blocked both Ca^{2+} oscillations and the rise in luminescence. Stopping ongoing Ca^{2+} oscillations at fertilization by chelation of extracellular Ca^{2+} caused a decline in ATP back to prefertilization levels (n=11). Furthermore, ATP increases could be stimulated by stimuli that cause Ca^{2+} oscillations such as addition of extracellular carbachol, or intracellular injection of PLCzeta cRNA. Repetitive Ca^{2+} increases could also be induced by pulses of UV light delivered to eggs that had been injected with caged InsP3 (Jones & Nixon, 2000). Such repetitive InsP3-induced Ca^{2+} increases stimulated at intervals of 10 min or 5 min resulted in a slow rise in luciferase luminescence (114±7.9%, n=6, and 119±8.7%, n=10, respectively). However, Ca^{2+} transients induced by InsP3 uncaging at intervals of 2.5 min resulted in a decrease in luciferase luminescence (-14.5±5.9%, n=8). These data suggest that Ca^{2+} oscillations at fertilization cause a net rise in ATP that starts with the first Ca^{2+} transient.

Dumollard R et al. (2004). Development 131, 3057-3067.

Jones KT & Nixon V (2000). Dev Biol 225, 1-12.

Stricker SA (1999). Dev Biol 211, 157-176.

This work was funded by the Wellcome Trust and K.C. is funded by the School of Medicine at Cardiff University.

Where applicable, the authors confirm that the experiments described here conform with the Physiological Society ethical requirements.

PC178

The mitogen lysophosphatidic acid produces Ca^{2+} signals in mouse embryonic stem cells

M.G. Todorova, I. Quesada, A. Nadal, E. Fuentes and B. Soria

Institute of Bioengineering, Miguel Hernandez University, Sant Joan d'Alacant, Spain

Lysophosphatidic acid (LPA) is one of the major mitogens found in blood serum. This bioactive phospholipid mediates various cellular responses through G-protein coupled transmembrane receptors. In many cell types LPA is known to trigger an increase in intracellular Ca^{2+} concentration, which is involved in the regulation of cell proliferation. The control of the proliferative state in embryonic stem (ES) cells is of high significance in view of their potential clinical use. However, the signalling pathways involved in the maintenance of this state are still not fully understood. In the present study we investigated whether LPA, as an extracellular molecule, provoked an effect on Ca^{2+} mobilization in D3 mouse ES cells and studied the molecular mechanisms involved. Using the Fura-2 fluorescence technique we demonstrated that indeed LPA over the range of 100 nM to 10 μM activates Ca^{2+} signalling in 96% of the mouse ES cells examined (n=28 experiments). This Ca^{2+} signal was mediated by mobilization from internal stores given that Ca^{2+} release was reproduced in the absence of extracellular Ca^{2+} (n=10 experiments). Consisting with this finding, treating the cells with 1μM thapsigargin, an inhibitor of the endoplasmic reticulum (ER) Ca^{2+} ATPase, completely abolished the LPA-stimulated Ca^{2+} increase in 3 out of 4 assays. Furthermore, we confirmed that in this LPA-induced Ca^{2+} mobilization the inositol 1,4,5-triphosphate (InsP3) activation was involved as the specific phospholipase C (PLC) inhibitor U73122 (3 μM) completely attenuated the increase in calcium concentration (n=6). On the contrary, the inactive analogue U-73343 applied at the same concentration (3 μM) did not produce any effect (n=4). In addition, we saw that LPA effect could be exerted through at least two types of receptors, LPA-1 and LPA-2 whose mRNAs were detected by RT-PCR assays (n=4). On a next stage we shall focus on the effect of this calcium mobilization on ES cell proliferation, investigating the molecular mechanisms involved. The basic research in the area of stem cells will contribute to a better understanding of their proper characteristics and signal pathways, as well as proliferation and differentiation processes assuring their better clinical application.

This work was supported in part by Grants from MCyT (GEN 2001-4748-CO5-05; SAF2004-07483-C04-01) and Instituto Carlos III (GO3/171; GO3/210; GO3/212) to B.S. and from MEC

(BFU2004-07283) to I.Q.

Where applicable, the authors confirm that the experiments described here conform with the Physiological Society ethical requirements.

PC179

Effects of extracellular ATP on Ca^{2+} signalling in mouse pancreatic alpha-cells

E. Tudurí and I. Quesada

Institute of bioengineering, Miguel Hernández University, Sant Joan d'Alacant, Spain

The hyperglycaemic hormone glucagon, which is released from pancreatic islet alpha-cells, plays a critical role in the maintenance of blood glucose homeostasis. Several factors including nutrients, circulating hormones and neurotransmitters control glucagon secretion. The secretory process in these endocrine cells is triggered by a rise in intracellular calcium concentration ($[Ca^{2+}]_i$). In the present study, we have investigated the effects of the neurotransmitter and beta cell secretory product ATP on the Ca^{2+} signalling system of mouse alpha-cells within intact islets using confocal microscopy (1). Data were expressed as means ± SEM. Statistical significance was analysed using a Student's t test ($p<0.05$). All cases were found significant.
Hypoglycaemic conditions (0.5 mM glucose), which stimulate glucagon secretion, induced oscillatory Ca^{2+} signals in alpha cells with a frequency of about 0.9 min^{-1}. Addition of 100 μM of ATP markedly inhibited these low glucose-induced Ca^{2+} signals (62.3 ± 7.5% blockade, n=19). These results were reproduced in the presence of clonidine (70.7 ± 9.4%, n=11), a potent inhibitor of insulin release, suggesting that the effects on alpha-cells were not due to paracrine stimulation from neighbouring beta-cells. The inhibitory effects were also generated by both ADP and adeno-

sine (68.5 ± 7.5%, n=24; 75.7 ± 5.8%, n=23, respectively), products resulting from ATP hydrolysis by ectonucleotidases, and by the non-hydrolysable ATPγS and ADPβS (29.7 ± 5.3%, n=8; 49.9 ± 6.1%, n=22, respectively), indicating thus, the potential involvement of multiple P1 and P2 receptors (2). Because no $[Ca^{2+}]_i$ elevations derived from Ca^{2+} influx were monitored during ATP stimulation, we ruled out the presence of functional P2X receptors. While ATP stimulation in the beta-cell triggers Ca^{2+} release from intracellular stores via phospholipase C activation, we discarded this possibility in alpha-cells because any $[Ca^{2+}]_i$ rise was detected. We also explored the involvement of adenylyl cyclase since the effect of multiple purine receptors is mainly mediated by changes in the cAMP levels, and this signalling molecule has an important effect on alpha-cell Ca^{2+} signalling. The addition of the adenylyl cyclase inhibitor 2',5'-dideoxyadenosine mimicked the effects of ATP on $[Ca^{2+}]_i$ signals (63.2 ± 7.7%, n=19). All these results suggest that ATP is a potent inhibitor of Ca^{2+} signalling in pancreatic alpha-cells, implicating the activation of multiple P1 and P2Y receptors coupled to G proteins. Although a further characterisation of the potential mechanism is required, the signalling pathway probably involves changes in cytoplasmic cAMP levels.

Nadal A, Quesada I & Soria B (1999). J Physiol 517, 85-93.

Ralevic V & Burnstock G (1998). Pharmacol Rev 50, 413-492.

This work was supported by grant BFU2004-07283 to I.Q.

Where applicable, the authors confirm that the experiments described here conform with the Physiological Society ethical requirements.

PC180

Inhibition of inositol 1,4,5-trisphosphate ($InsP_3$)-induced calcium release (IICR) by the calcium binding protein calmyrin

A.M. Holmes[1], N. Kasri[3], H. De Smedt[3], J. Parys[3], F. McDonald[2], M. Bootman[1] and H.L. Roderick[4]

[1]Calcium Group, Babraham Institute, Cambridge, UK, [2]Department of Orthodontics and Paediatric Dentistry, UMDS, London, UK, [3]Laboratorium voor Fysiologie, K. U. Leuven, Leuven, Belgium and [4]Department of Pharmacology, University of Cambridge, Cambridge, UK

Inositol 1,4,5-trisphosphate receptors ($InsP_3Rs$) are widely-expressed intracellular channels that release Ca^{2+} from internal stores in response to many physiological stimuli. It is becoming apparent that $InsP_3Rs$ form complexes with a multitude of accessory proteins. Many of the proteins that bind to $InsP_3Rs$ appear to modulate channel function and Ca^{2+} release.

$InsP_3Rs$ are known to be regulated by the ubiquitous EF-hand Ca^{2+}-binding protein calmodulin (CaM). We recently demonstrated that members of the neuronal 'calcium binding protein' family (CaBPs), which also bind Ca^{2+} using EF-hand motifs and have approximately 50% homology with CaM, functionally interact with $InsP_3$ receptors ($InsP_3R$) and inhibit IICR (1). In the present study, we examined the putative interaction of another EF-hand-containing protein, calmyrin, which is ubiquitously expressed and has 56% homology to CaM.

We found that calmyrin interacts with the NH_2-terminus of $InsP_3Rs$ in a Ca^{2+}-independent manner (n=3). Video imaging of fura-2 loaded COS7 cells over-expressing YFP-tagged calmyrin revealed that calmyrin inhibited Ca^{2+} release from internal stores induced by purinergic agonist (ATP; 0.5, 1 and 100 μM) (refer to table 1 for percentage of responding cells, peak amplitude of the response and integrated response). A mutated protein in which the consensus site for myristoylation was altered ('calmyrin-G2A') also inhibited IICR. Unlike wild-type calmyrin, which was largely bound to cellular membranes, the calmyrin-G2A mutant was diffuse. From these data we concluded that calmyrin function is not dependent on its myristoylation and hence membrane targeting. Recombinant calmyrin also inhibited $InsP_3$-dependent $^{45}Ca^{2+}$ flux from permeabilised cells (the IC_{50} of IICR increased from 0.45 ± 0.06 μM to 0.87 ± 0.07 μM in the presence of 10 μM calmyrin (n=3)). The calmyrin-mediated inhibition of Ca^{2+} release was $InsP_3R$ specific since there was no inhibition of caffeine-induced Ca^{2+} release from ryanodine receptors (peak amplitude of response to 0.5 mM caffeine: 59 ± 8.05 nM (n=10 calmyrin-expressing cells) vs. 67.5 ± 4.69 nM (n=42 control cells); p>0.01). To investigate the mechanism by which calmyrin mediates its effect we performed an $InsP_3$ binding assay using recombinant $InsP_3R$ ligand binding domain. In these studies we demonstrated that calmyrin inhibited $InsP_3$ binding to the $InsP_3R$ by 22 ± 3% (n=3), in a Ca^{2+}-independent manner.

Our data indicate that calmyrin interacts with $InsP_3Rs$ and inhibits IICR in a similar manner to CaBPs and CaM.

Table 1. Inhibition of IICR in COS7 cells stimulated with ATP

	Responders (%)			Peak amplitude (nM)			Integrated response ($nMs^{-1} x10^4$)		
ATP (μM)	0.5	1	100	0.5	1	100	0.5	1	100
Control	89.9 ± 1.29	100	100	178.6 ± 11.5	263.1 ± 10.7	403.0 ± 10.6	0.8 ± 0.04	1.31 ± 0.04	2.01 ± 0.04
Calmyrin	21.3 ± 5.43	76.0 ± 2.1	100	49.8 ± 16.4	152.1 ± 11.3	320.4 ± 11.5	0.2 ± 0.04	0.5 ± 0.03	1.74 ± 0.06

Kasri NN, Holmes AM, Bultynck G, Parys JB, Bootman MD, Rietdorf K et al. (2004). Embo J 23, 312-321.

Where applicable, the authors confirm that the experiments described here conform with the Physiological Society ethical requirements.

PC181

The relationship between GSH level and compartimentation, telomerase activity and Bcl-2 expression in human mammary carcinoma cell lines Mcf7- and Mcf7+

J. Markovic, C. Borras, A. Ortega, N. Mora, A. Broseta, F.V. Pallardo and J. Viña

Physiology, University of Valencia, Valencia, Spain

It has been proposed that cancer originates from a rare coincidence where the cell acquires simultaneously deregulated proliferation and suppressed apoptosis (1). The importance of GSH in the pathology of cancer has long been recognized, as well as

its central place in the control of vital cell processes of great diversity including cell proliferation (2). Bcl-2, the antiapoptotic protein, promotes the compartimentation of the GSH in the nucleus and thus contributes to the resistance to apoptosis (3). Considering the growing evidence that shows the importance of GSH compartimentation, and its role in numerous processes that occur in the nucleus, we have studied the changes in the GSH distribution throughout the cell cycle in MCF7- (Bcl-2 wild type +/-), and its Bcl-2 over expressing analogue, MCF7+ (Bcl2+/+) in order to see the possible relation between Bcl-2, GSH level, telomerase activity (TA) and cell proliferation.

We studied the cell cycle by flow cytometry, total GSH (GSHt) level by spectrophotometry, telomerase activity by TRAP assay and its distribution by confocal microscopy. Triple staining was applied: propidium iodide (PI) to identify dead cells, Hoechst to localize nucleus and CellTracker green 5-chloromethylfluorescein diacetate (CMFDA), which marks GSH (specificity 95%).

Our results show that the peak of GSHt in MCF7+ is at 6h (304.9 ±1 8.5 nmol/mg prot, $p<0.001$ vs 12h) and precedes the peak of TA at 12h (2220 ± 754), while in MCF7- both GSHt (256.8 ± 61.1 nmol/mg prot, $p<0.05$ vs 24h) and TA (1448 ± 522) have their maximum at 18h after plating. MCF7+ cells show significantly higher level of GSHt and TA. By confocal microscopy we observed a growing tendency of GSH compartimentation in the nucleus of both cell types starting from 24h of culture which coincides with the plateau of high cell proliferation rate and is maintained until 72h after plating.

We demonstrate that the level of GSH and TA in MCF7 cells could be, at least in part, Bcl-2 dependent. However, there was no significant difference in GSH distribution or in cell cycle dynamic and proliferation rate between MCF7+ and MCF7- cells.

Green & Evan (2002). Cancer Cell 1, 19-30.

Jones DP et al. (2002). Methods Enzymol 348, 93-112.

Voehringer DW et al. (1998). Proc Natl Acad Sci USA Cell Biol 95, 2956-2960.

Where applicable, the authors confirm that the experiments described here conform with the Physiological Society ethical requirements.

PC182

Induction of apoptosis by glutamine and serum deprivation in 3T3 fibroblast. Cell cycle and GSH compartimentation relationship

N.J. Mora, J. Markovic, A. Ortega and F.V. Pallardo

Physiology, University of Valencia, Valencia, Spain

The glutamine (Gln) has been termed 'conditionally essential' because is often depleted during times of catabolic stress like cancer, severe infection (sepsis) and burn injury. This characteristic depletion is attributed to its role as a metabolic intermediate aporting carbon and nitrogen for the synthesis of other amino acids, fatty acids, nucleic acids and proteins and also supplying a source of fuel for dividing cells. Gln is an essential component of glutathione (GSH) homeostasis. GSH is the primary intracellular antioxidant, scavenger of free radicals, peroxides and other reactive species. As a consequence of their exhaustion the process of apoptosis is triggered. Gln deprivation ultimately elicits apoptosis by intrinsic and/or extrinsic pathways, depending on the cell type (1). The aim of these work was to assess the glutamine and serum deprivation effects on the cell cycle and GSH compartimentation. Cells was cultured in DMEM media supplemented with 10% fetal calf serum (FCS) using $2x10^5$ cells cm^2, and grown at 37°C in a humidified atmosphere of 5% CO_2 air mixture for 24 h. To induced apoptosis cultured medium was removed and the cells were cultured in Gln, serum and Gln-serum deprived medium for 48 h. In control cells medium was changed too. Cells were treated with propidium iodide (IP), to identify dead cells, and annexine V, for apoptosis measurement, then the of apoptosis and cells cycle were determined by flow cytometry. The GSH levels were determined by spectrophotometry. To visualize GSH localization, cells were observed with a Leica confocal microscope. Triple staining was applied: propidium iodide (Hoechst; 2 mg/ml) to localize nucleus and CellTracker green 5-chloromethylfluorescein diacetate (5mM; CMFDA), which marks GSH (specificity 95%).

Our results show that the cell death and apoptosis levels are higher in the conditions of Gln deprivation, than in serum-deprived cells and control (33.6±3.41; 23±1.9 and 7.45±1.6, $p<0.05$, respectively). Also GSH levels in these cells were significantly lower compared with control cells and serum-deprived cells (73±28, 95±29.3 and 46±12.6 nmol/mg prot, $p<0.05$, respectively). By confocal microscopy we observed that serum deprivation caused nuclear GSH compartimentation, while in Gln-deprived cells the GSH distribution was homogeneous.

Our results suggest that those cells with higher nuclear GSH levels are more resistant to apoptosis.

Fuchs BC & Bode BP (2006). J Surg Res 131, 26-40.

Where applicable, the authors confirm that the experiments described here conform with the Physiological Society ethical requirements.

PC183

Glutathione level and cell cycle relationship in embryonic cultures of Wistar rat neurons

J. Markovic, N. Mora, S. Ballester, P. Martin, A. Ortega, A. Broseta and F.V. Pallardo

Physiology, University of Valencia, Valencia, Spain

Reduced glutathione (GSH) is a low molecular weight thiol and the most abundant non-enzymatic antioxidant in the cell. Its property to maintain cellular thiol/disulfide redox state gives it a central place in the control of great diversity of vital cell processes including cell proliferation (1).

Our group has recently investigated the possible relationship between telomerase activity and cellular GSH concentration and we have demonstrated that the peak of total GSH (tGSH) in 3T3 fibroblasts coincides with the peak of telomerase activity (TA) at 24h in culture preceding the exponential phase of the cell growth (2).

The objective of the present work was to analyse the relation between GSH levels and cell cycle in a non-proliferative cell model. We chose rat embryonic neurons that once diferentiated do not have mitotic activity.

Primary cultures were established of neurons from the cerebral cortex of fetal Wistar rats (gestation day 14) (3). To prevent non-

neuronal proliferation 20 μM cytosine arabinoside (AraC) was added on the 4th day of culture, and 24h afterwards half of the culture medium was changed. Until the 18th day of culture we studied the cell cycle by flow cytometry, GSH levels by spectrofotometry and cell viability by double staining propidium iodide (PI; 2μg/ml) to identify dead cells and Hoechst (2μg/ml) to localize all the nuclei. The level of glial contamination was defined by inmunocitochemistry and was less than 3%.
In the first 4 days of culture, before the AraC was added, the peak of GSH at 48h (39.6±4.6 nmol/mg prot, $p<0.01$ and $p<0.05$ vs 3h and 7 days, respectively) was followed by the maximum proliferation at 72h (S+M/G2=15±1.1, $p<0.01$ vs. 5.7±0.3 at 7 days). After the AraC was added, the cell culture stabilized in G0/G1 (39.2± 0.7%) and the level of GSH dropped significantly (27.9±2.5 nmol/mg prot at 7 days). A higher percentage of cell death could be attributed to the elimination of non-neuronal cells by AraC.
Our results show that while freely proliferating, the primary culture of cerebral cortex demonstrates the same tendency as in 3T3 fibroblasts (2). The GSH maximum level preceeds the peak of proliferation. However, in a 97% pure neuronal culture, when the non-neuronal cells were eliminated, the level of GSH and proliferation is significantly lower and it remains stable throughout the period of culture.

Jones DP et al. (2002). Methods Enzymol 348, 93-112.

Borrás C et al. (2004). J Biol Chem 279, 34332-3435.

Brewer GJ et al. (1997). J Neurosci Methods 71, 143-155.

Where applicable, the authors confirm that the experiments described here conform with the Physiological Society ethical requirements.

PC184

Wheat germ agglutinin holds nuclear pores of chick embryo sensory neurones open for calcium diffusion

E. Aslim and S.R. Bolsover

UCL, London, UK

Although calcium is thought to equilibrate across the nuclear envelope, the envelope nevertheless represents a significant barrier to rapid diffusion. We have investigated the delay to calcium diffusion caused by the nuclear envelope, and the effect of two agents on that delay: histone proteins, which will be actively transported by the pore complex, and wheat germ agglutinin, which inhibits active pore transport.
Cultured sensory neurones of 12 day old chick embryos replated onto a polyornithine substrate on the day before experimentation displayed a simple ovoid shape without neurites. Immediately before experimentation nuclei were stained with 2 μM Hoechst 33342. The bathing medium was then switched to 120 mM NaCl, 1.2 mM $MgCl_2$, 5.5 mM KCl, 1.8 mM $CaCl_2$, 1.8 mM TEACl, 10 mM HEPES, 25 mM glucose, 1 μM tetrodotoxin and 5 μM (S)-(-)-BAY K 8644, pH 7.2. The presence of BAY K enhanced calcium currents and therefore increased the depolarization-evoked fluorescence signal. Neurons were whole cell patch clamped, at room temperature, on the stage of a Zeiss 510 confocal microscope through pipettes containing 125 mM CsCl, 4 mM MgATP, 10 mM HEPES and 100 μM of the calcium indicator Oregon Green BAPTA 488 Dextran, 10 kD, pH 7.2, plus 500 μg/ml of a histone mixture (Sigma H-7755) or 100 μg/ml of wheat germ agglutinin (Sigma L-9640) as appropriate.
Neurones were held in whole cell mode for 3 min to allow diffusion of the dye and active agents into the cytosol and to the nuclear pores. Neurones were then scanned every 1.92ms along a line that passed through the nucleus (excitation 488 nm, emission >505 nm, confocal plane 3 μm). Depolarization (-70 mV to +10 mV for 50 ms) evoked a calcium increase that could be seen to pass from the cell edge to the cell centre within tens of milliseconds. Comparing the rising phase of the fluorescence signal in the nucleus, and at the same distance from the cell edge in the cytosol, yielded a value for the delay due to the nuclear envelope. In control cells this was 6.2 ± 2.7 ms (± SEM, N=10). In the presence of histone mixture the value was not significantly different (6.6 ± 4.7 ms, N=9). However, wheat germ agglutinin eliminated the delay (time difference -1.1 ± 2.1 ms, N=12). The last value is not significantly different from zero, but is significantly different (P<5%, t test) from the control value.
Our tentative interpretation is that in control cells the majority of the nuclear pores are transporting macromolecular cargo, so that addition of extra cargo in the form of histone has little effect on the average pore topology. Wheat germ agglutinin inhibits the binding and transport of macromolecules so that the entire diameter of all the nuclear pores is available for calcium diffusion.

Where applicable, the authors confirm that the experiments described here conform with the Physiological Society ethical requirements.

PC185

SNAP-25 is a novel inositol 1,4,5-trisphosphate receptor ($InsP_3R$) interacting protein that regulates intracellular Ca^{2+} release and influx

K. Rietdorf[2], J. Webster[3], D. Oxley[3], M.D. Bootman[2] and H.L. Roderick[1]

[1]Pharmacology, University of Cambridge, Cambridge, UK, [2]Molecular Signalling, Babraham Institute, Cambridge, UK and [3]Protein Technologies, Babraham Institute, Cambridge, UK

Inositol 1,4,5-trisphosphate receptors ($InsP_3Rs$) are major intracellular Ca^{2+} release channels in non-excitable cells. In addition to regulation by $InsP_3$ and Ca^{2+}, they are modulated by post-translational modification and the binding of accessory proteins. Thus, $InsP_3Rs$ act as scaffolds, anchoring many signalling proteins to the site of Ca^{2+} release, where they either regulate, or are regulated by Ca^{2+} release through the channel (1). To identify novel $InsP_3R$ interacting proteins, a proteomic approach was used. To this end, $InsP_3Rs$ were immunoprecipitated from rat brain lysate, which is a rich source of type 1 $InsP_3Rs$. Co-immunoprecipitated proteins were subsequently eluted and subjected to 2-dimensional liquid chromatography and Matrix Assisted Laser Desorption Ionization Time-of-flight Mass Spectrometry analysis (MALDI-TOF). Using this strategy, we identified the SNARE-associated protein SNAP-25. This interaction was confirmed by subsequent immunoblotting of proteins co-immunoprecipitated with the $InsP_3R$ (n>3). SNAP-25 is a protein involved in Ca^{2+}-regulated secretory processes and associates with N- and P/Q-type voltage-operated plasma membrane Ca^{2+}-channels.

To test whether the expression of SNAP-25 affects Ca^{2+} signalling, we established stable HeLa cell lines that expressed YFP-SNAP-25 in a tetracycline-inducible manner. In these cells, YFP-SNAP-25 was targeted to the plasma membrane. Using fura-2 imaging, we investigated whether overexpression of YFP-SNAP-25 affected $InsP_3$-induced Ca^{2+} release and store operated Ca^{2+} entry. Cells overexpressing YFP were used as control. Experiments were performed on at least two different days and on three coverslides for each cell line per day. Statistical significance was determined by a Mann-Whitney U test. Data are presented as mean±SEM.

To investigate the effect of SNAP-25 on $InsP_3$-induced calcium release, cells were stimulated with increasing doses of the $InsP_3$-generating agonist histamine (0.5, 1 and 100 μM). Cells overexpressing YFP-SNAP-25 exhibited decreased Ca^{2+} responses to all concentrations of histamine applied (78.6±5.7%, 74.5±6.5%, and 73.3±1.7%, $p<0.01$ for all three concentrations).

The rate of quench of cellular fura-2 fluorescence by Mn^{2+}, which was used as Ca^{2+} surrogate in these experiments, was used to measure the effects of SNAP-25 on Ca^{2+} entry. In the YFP-SNAP-25 overexpressing cells, basal and histamine-induced Ca^{2+} entry (100 μM histamine for 10 min) was significantly greater than in YFP-expressing control cells (241.9±17.2% and 357.3±12.8% respectively, both $p<0.0001$). The SNAP-25-enhanced Ca^{2+} entry was inhibited by 1 μM Gd^{3+}, indicating that it occurred via the store-operated Ca^{2+} entry (SOCE) pathway. In summary, we have shown that SNAP-25 is a novel $InsP_3R$ interacting protein, which affects both Ca^{2+}-release from the ER and SOCE.

Roderick HL & Bootman MD (2003). Biochem Soc Trans 31, 950-953.

Where applicable, the authors confirm that the experiments described here conform with the Physiological Society ethical requirements.

PC186

Genetic iron overload versus dietary iron overload in SWR mice

M. Mascarenhas[1], K.S. Srai[1] and R. Simpson[2]

[1]Biochemistry & Molecular Biology, Epithelial Transport and Cell Biology Group (ETCBG), University College London (Hampstead Campus), London, UK and [2]Life Sciences, King's College London, London, UK

Hereditary haemochromatosis is an autosomal recessive disorder of iron (Fe) metabolism and a mutation in the Hfe gene is the most common cause of the disease. Haemochromatosis is characterised by defective regulation of dietary iron absorption that leads to excessive Fe accumulation in various organs including the liver, pancreas, heart, joints, and pituitary gland leading to hepatic cancer, liver failure, diabetes, and heart disease. Recent findings suggest hepcidin, a hormone produced by the liver, is a negative regulator of Fe absorption and is itself regulated by iron, anaemia, hypoxia and inflammation. In the case of haemochromatosis expression of hepcidin is inappropriate for the levels of liver Fe and this leads to increased Fe uptake despite liver iron being elevated. These observations are based on measurement of iron and hepcidin expression in biopsies or a part of a lobe; however, there is no information on Fe levels or hepcidin expression in relation to different lobes in the liver.

The aim of this study was to investigate the level of Fe in each lobe of the liver and measure the hepcidin gene expression in SWR-wild type (wt) and SWR-Hfe knockout mice.

Both wt and Hfe knockout mice were studied at the age of 12 weeks. The livers were divided into five lobes and named A to E, Fe quantification was done by the Torrance and Bothwell method and hepcidin gene expression was measured by RT-PCR.

We found that in SWR wt mice liver Fe in all the lobes ranged from 70 to 90 μg/g dry weight (79.8±5.1 μg/g dry weight). In SWR Hfe knockout mice, liver Fe levels were higher as expected and in lobes B to E Fe levels ranged from 350 to 500 μg/g dry weight (438±15.6 μg/g dry weight). Interestingly, lobe A had a much higher level of Fe than any of the other lobes (821.6±102.8 μg/g dry weight, n=8). When hepcidin 1 gene expression levels were measured, there was no difference between the different lobes in the SWR wt mice (Table 1), but in the SWR Hfe knockout mice, although the hepcidin levels were lower than the wt, there were differences between the lobes, lobe A being the one with the highest level of hepcidin expression.

When SWR wt mice were fed a high Fe diet, although there was a great accumulation of Fe in the liver, no differences were seen between the lobes (Table 2).

In conclusion, the Hfe gene seems to cause a preferential accumulation of Fe in the specific lobes of the liver. Furthermore hepcidin expression was highest in the lobe with the highest Fe levels. This suggests that liver Fe levels regulate hepcidin but this regulation is perturbed by Hfe. This finding is also relevant to the diagnosis of haemochromatosis as the common practice is to perform biopsies of a particular region of the liver and this might not correspond to the actual Fe accumulation status of the liver.

Table 1. Hepcidin 1 mRNA content relative to actin, in the different liver lobes of SWR wt (n=5) and Hfe knockout (n=5) fed on a normal diet

Lobe	SWR wt (hepcidin 1 expression)	SWR Hfe KO (hepcidin 1 expression)
A	0.23±0.06	0.18±0.10
B	0.21±0.03	0.04±0.03
C	0.37±0.07	0.04±0.005
D	0.12±0.02	0.06±0.03
E	0.12±0.02	0.02±0.01

Values are mean±SEM.

Table 2. Liver irons (μg/g dry weight) of the different lobes in SWR wt fed an high iron diet (n=6)

Lobes	SWR wt on high iron diet (μg/g dry weight)
A	578.8±107.8
B	484.7±52.4
C	512.7±85.4
D	514.3±104.4
E	527.8±79.3

Values are mean±SEM.

Where applicable, the authors confirm that the experiments described here conform with the Physiological Society ethical requirements.

PC187

Adhesion of human breast cancer cell lines: role of voltage-gated sodium channel β1 subunit

A. Chioni[1], L. Isom[2] and M.B. Djamgoz[1]

[1]Cell & Molecular Biology, Imperial College London, London, UK and [2]Pharmacology, The University of Michigan, Ann Arbor, MI, USA

Voltage-gated Na^+ channel (VGSC), predominantly neonatal Nav1.5 (nNav1.5), expression is upregulated in metastatic breast cancer (BCa) and VGSC activity potentiates a variety of metastatic cell behaviours (Fraser et al. 2005). VGSCs incorporate one or more β-subunit (VGSCβ) which can modulate channel gating and functional expression (Chen et al. 2002). Interestingly, VGSCβ's can also serve as cell adhesion molecules by interacting with extracellular matrix proteins and cytoskeleton (Isom, 2002). The aims of the study were (1) to determine which VGSCβ's were expressed in weakly and strongly metastatic human BCa (MCF-7 and MDA-MB-231, respectively) cell lines and (2) to test the possible role of VGSCβ expression in cellular adhesion and migration.

MCF-7 and MDA-MB-231 cells were cultured (Fraser et al. 2005). Real-time PCR and Western blot (WB) with a polyclonal antibody specific for β1 (Malhotra et al. 2000) were used to study and quantify gene and protein expression. Transwell migration and adhesion were measured as before (Fraser et al. 2005; Aydar et al. 2006). A small interfering RNA (siRNA) technique was used to silence specifically the β1 gene in MCF-7 cells; the control transfection involved a scrambled siRNA (siControl). Data (mean ± SEM) were analysed by paired t tests, unless otherwise stated.

Real-time PCR revealed that in both MCF-7 and MDA-MB-231 cell lines, VGSCβ expression profile was as follows: β1>> β4> β2 (β3 was absent). MCF-7 cells had a much higher overall level of VGSCβ mRNA expression, compared to MDA-MB-231. WBs verified that β1 protein was strongly expressed in MCF-7 and barely detectable in MDA-MB-231 cells. In siRNA-transfected MCF-7 cells, β1 mRNA (normalised to cytochrome b5 reductase) was reduced by 76 ± 4% after 4 days, relative to siControl ($P<0.01$; n=3). Protein-level reduction (normalised to actin) was less pronounced, only 39 ± 7% after 8 days ($P<0.01$; n=11). Under control conditions, MCF-7 cells were much more adhesive than MDA-MB-231 cells, in line with their weak metastatic potential. However, 8 days after β1 siRNA transfection, the adhesion of MCF-7 cells was reduced by 34 ± 2% ($P<0.001$; n=6). Interestingly, concurrently, the cells' migratory activity increased by 121 ± 14% compared to siControls ($P < 0.05$; n = 8). This increase was largely dependent upon VGSC activity since application of TTX (10 microM) to siRNA-treated cells reduced migration to the control level ($P= 0.4$ for siRNA vs siControl, both treated with TTX; n=8). Indeed, in siRNA-treated MCF-7 cells, nNav1.5 mRNA and protein levels were significantly higher.

We conclude (1) that VGSCβ1 subunit expression makes a significant contribution to the strong adhesiveness of the weakly metastatic MCF-7 cells and (2) that VGSCβ1 downregulation would increase migration via VGSC expression/activity.

Aydar E et al. (2006). Cancer Letters (in press).

Chen C et al. (2002). Proc Natl Acad Sci USA 99, 17072-17077.

Fraser SP et al. (2005). Clin Cancer Res 11, 5381-5389.

Isom LL (2002). Front Biosci 7, 12-23.

Malhotra JD et al. (2000). J Biol Chem 275, 11383-11388.

This study was supported by an Amber Fellowship (PCRF) to A-M.C.

Where applicable, the authors confirm that the experiments described here conform with the Physiological Society ethical requirements.

PC188

Role of phospholipases in store-operated Ca^{2+} entry in human platelets

M.T. Harper and S.O. Sage

Department of Physiology, Development & Neuroscience, University of Cambridge, Cambridge, UK

Store-operated Ca^{2+} entry (SOCE) is a major pathway for Ca^{2+} entry in human platelets, although the mechanism of SOCE activation has not been clearly established. In one model, Ca^{2+} store depletion induces *de novo* conformational coupling of the type II IP_3 receptor to hTRPC1, believed to be a component of the store-operated channel. This coupling requires basal levels of IP_3 and functional IP_3 receptors (1, 2). In contrast, an alternative model suggests that Ca^{2+} store depletion induces formation of a Ca^{2+} influx factor (CIF) that displaces calmodulin (CaM) from Ca^{2+}-independent phospholipase A_2 ($iPLA_2$), resulting in $iPLA_2$ activation and lysophospholipid production, which then activates the store-operated channel (3). Here the role of $iPLA_2$ in SOCE activation in human platelets has been investigated.

Fura-2–loaded human platelets were stimulated with the CaM inhibitor, calmidazolium (CMZ), resulting in a concentration-dependent increase in Ca^{2+} release and Ca^{2+} entry. At no concentration was Ca^{2+} entry seen without Ca^{2+} release. No Ca^{2+} entry was detected using 1 μM CMZ, and only a relatively small Ca^{2+} entry was detected using 10 μM. In contrast, $iPLA_2$ was strongly activated by 1 μM CMZ, and maximally activated by 10 μM. These data suggest that $iPLA_2$ activation in not sufficient for SOCE activation in these cells.

Thapsigargin-evoked SOCE was completely abolished by prior incubation with the iPLA2 inhibitor, bromoenol lactone (BEL; 25 μM; 30 min). BEL was found to increase resting intracellular Ca^{2+} concentration from 61 ± 4 nM to 155 ± 2 nM (mean ± SEM; n = 6; $p < 0.005$; Student's t test). BEL also reduced PAR-1 –dependent Ca^{2+} release to 20.2 ± 2.1% of control (n = 6; $p < 0.005$), which appeared to be due to inhibition of agonist-evoked IP_3 synthesis. IP_3 levels in cells stimulated by the PAR-1 agonist, SFLLRN, after BEL treatment were not significantly higher than basal (100.9 ± 10.2% of control; n = 6; $p = 0.48$), as measured by a fluorescence polarisation assay.

Inhibition of phospholipase C by Et-18-OCH_3 also significantly inhibited TG-evoked SOCE to 12.7 ± 3.6% of control (n = 9; $p < 0.001$). This is consistent with an essential role for basal IP_3 in the activation of SOCE (1). The disruption of IP_3 production

by BEL may be owing to the role of $iPLA_2$ in remodelling of the fatty-acid content of membrane phospholipids.
In conclusion, although $iPLA_2$ appears to have an important role in regulation of cell signalling through the remodelling of cellular phospholipids, it is unlikely to play a direct role in SOCE activation in human platelets.

Rosado JA & Sage SO (2000). *Biochem J* **350**, 631-635.

Rosado JA & Sage SO (2001). *Biochem J* **356**, 191-198.

Smani *et al.* (2003). *J Biol Chem* **278**, 11909-11915.

Supported by the British Heart Foundation.

Where applicable, the authors confirm that the experiments described here conform with the Physiological Society ethical requirements.

PC191

Transforming growth factor-β1 induces heme oxygenase-1 in human aortic smooth muscle cells: role of Nrf2, mitogen-activated protein kinases and superoxide generation

R.C. Siow, A.A. Anwar and G.E. Mann

Cardiovascular Division, Kings College London, London, UK

Reactive oxygen species contribute to atherogenesis resulting from endothelial and smooth muscle dysfunction. We have previously reported that oxLDL induces the expression of the antioxidant-like stress protein heme oxygenase-1 (HO-1) in human aortic smooth muscle cells (HASMC, Anwar *et al.* 2005). HO-1 catabolises the pro-oxidant heme to the antioxidants biliverdin and the vasodilator carbon monoxide (Siow *et al.* 1999). Transforming growth factor-β1 (TGF-β1) stimulates vascular SMC growth and extracellular matrix synthesis which contributes to vascular remodelling (Topper, 2000). Induction of cytoprotective antioxidant genes such as HO-1 is regulated by the transcription factor Nrf2 and act to limit oxidative injury (Ishii *et al.* 2000). We have now investigated whether TGF-β1 activates Nrf2 to mediate HO-1 induction and the involvement of mitogen-activated protein kinases (MAPK) and free radical generation in human aortic SMC. Cells were treated with TGF-β1 (0–10 ng/ml, 0–24 h) and HO-1 expression and phosphorylation of extracellular signal-regulated kinase (ERK1/2), $p38^{MAPK}$ and c-Jun N-terminal kinase (JNK) determined by western blot analyses. Activation of Nrf2 translocation was determined by immunofluorescence and immunoblot analyses of nuclear lysates. NADPH-dependent superoxide generation was assessed by lucigenin chemiluminescence in cell homogenates. The statistical signigficance of quantified data were evaluated using Student's unpaired t tests.
TGF-β1 (2.5 ng/ml, 2 h) treatment led to nuclear translocation of Nrf2, phosphorylation of JNK, $p38^{MAPK}$ and ERK1/2, and increased superoxide production by 1.5±0.2-fold (mean±SEM, $n = 3$, $p<0.01$). Pretreatment of cells with apocynin (100 μM), an NADPH oxidase inhibitor, significantly attenuated superoxide generation elicited by TGF-β1 by 34±8% ($p<0.05$, $n=3$). HO-1 expression was enhanced by TGF-β1 (2.5 ng/ml), reaching a maximum 10.3±2.3-fold increase between 8–12 h (mean±SEM, $n = 3$, $p<0.01$).
Modulation of TGF-β1-mediated Nrf2 activation, free radical production and HO-1 expression may provide mechanistic insights for the contribution of this growth factor to vascular disease processes.

Anwar AA *et al.* (2005). *Free Radic Biol Med* **39**, 227-236.

Siow RC *et al.* (1999). *Cardiovasc Res* **41**, 385-394.

Topper JN (2000). *Trends Cardiovasc Med* **10**, 132-137.

Ishii *et al.* (2000). *J Biol Chem* **275**, 16023-16029.

Supported by the Guy's & St Thomas' Charitable Foundation and the British Heart Foundation.

Where applicable, the authors confirm that the experiments described here conform with the Physiological Society ethical requirements.

PC191a

Activity of protein tyrosine phosphorylation enzymes in stomach mucosa cells of rats with stress-induced gastric lesions

O.V. Bogdanova, L.I. Kuzmenko, K.V. Prokopova, V.B. Bogdanov and L.I. Ostapchenko

Biochemistry, Taras Shevchenko Kyiv National University, Kyiv, Ukraine

(Title only)

Where applicable, the authors confirm that the experiments described here conform with the Physiological Society ethical requirements.